Structural Characterization of Self-Assembled MnO_2 Nanosheets from Birnessite Manganese Oxide Single Crystals

Xiaojing Yang,† Yoji Makita, Zong-huai Liu, Kohji Sakane, and Kenta Ooi*

National Institute of Advanced Industrial Science and Technology, 2217-14 Hayashi, Takamatsu 761-0395, Japan

Received June 18, 2004. Revised Manuscript Received September 17, 2004

We report in this paper the studies on protonation, exfoliation, and self-assembly of birnessite-type manganese oxide single crystals. The protonation was carried out by extracting K^+ ions from the potassium manganese oxide single crystals in a $(NH_4)_2S_2O_8$ aqueous solution heated at 60 °C, exfoliation to nanosheets by the intercalation of TMA^+ ions followed by water-washing, and the self-assembly of MnO_2 nanosheets in a dilute NaCl solution. The structures of the samples at these stages were systematically investigated using X-ray diffraction, scanning electron microscopy, transmission electron microscopy, atomic force microscopy, X-ray photoelectron spectroscopy, Fourier transform infrared, thermogravimetric analysis-differential thermal analysis, and chemical compositional analysis. Electron density distribution in the protonated single crystal was visualized by whole-pattern fitting based on the maximum entropy method. The results indicated that the protonated single crystals can be exfoliated to MnO_2 unilamellar nanosheets. The self-assembly yields layered crystals with basal spacing of 0.72 nm and with a composition of $H_{0.18}Na_{0.089}MnO_2 \cdot 0.47H_2O$. The layered crystals had a textured polycrystalline structure, where *c*-axes of the nanosheets aligning along a certain direction constitute a fiber axis with azimuthal orientations of *a*- or *b*-axes about the fiber axis. Moreover, the azimuthal orientations of *a*- or *b*-axes are probably arranged at particular angles to one another, rather than randomly. The mean oxidation state of manganese exhibits no marked change at the various stages of the protonation, exfoliation, and self-assembly.

Introduction

Self-assembly is one of the few practical strategies for making ensembles of nanostructures and, as a consequence, an essential part of nanotechnology.[1] Various materials consisting of interlayer nanocomposites of polymer or inorganic (poly)ions/layered hosts have been synthesized using the exfoliation (or delamination)/reassembly (or restacking) process. To prepare nanometer-size building blocks, conversion of inorganic layered materials to nanosheets by exfoliation has attracted strong interest. These layered materials include a wide variety of compositions and structures, such as layered silicate,[2] titanium dioxide,[3] zirconium phosphate,[4] double hydroxides,[5] perovskites,[6] graphite oxide,[7] and manganese oxide.[8,9] A typical example using the exfoliation/reassembly process is polymer-clay nanocomposites.[10] Suspensions or sols containing exfoliated nanosheets can be cast or spin-coated to form thin films[11] or thin flakes and hollow spheres.[12] A layer-by-layer method has been developed to prepare a more complex nanosystem.[13]

Manganese oxides find application as cathodes in lithium ion batteries,[14] oxidation catalysts,[15] and selective adsorbents[16] and exhibit giant or colossal magnetoresistance.[17] Nanometer-scale manganese oxides may

* To whom correspondence should be addressed. Telephone: +81-87-869-3511. Fax: +81-87-869-3551. E-mail: k-ooi@aist.go.jp.

† Present address: Advanced Materials Laboratory, National Institute for Materials Science, Namiki 1-1, Tsukuba, Ibaraki 305-0044, Japan. Telephone: +81-29-851-3354. Fax: +81-29-854-9061. E-mail: YANG.Xiaojing@nims.go.jp.

(1) Whitesides, G. M.; Grzyowski, B. *Science* **2002**, *29*, 2418.

(2) (a) Lerf A.; Schöllhorn, R. *Inorg. Chem.* **1977**, *16*, 2950. (b) Naadeau, P. H.; Wilson, M. J.; McHardy, W. J.; Tait, J. M. *Science* **1984**, *225*, 923. (c) Strawhecker, K. E.; Manias, E. *Chem. Mater.* **2000**, *12*, 2943.

(3) Sasaki, T.; Watanabe, M. M. *J. Am. Chem. Soc.* **1998**, *120*, 4682.

(4) Alberti, G.; Casciola, M.; Costantino, U.; Di Gregorio, F. *Solid State Ionics* **1989**, *32*, 40.

(5) Leroux, F.; Adachi-Pagano, M.; Intissar, M.; Chauviere, S.; Forano, C.; Basse, J.-P. *J. Mater. Chem.* **2001**, *11*, 105. (b) Leroux, F.; Besse, J.-P. *Chem. Mater.* **2001**, *13*, 3507.

(6) Schaak, R. E.; Mallouk, T. E. *Chem. Mater.* **2002**, *14*, 1455.

(7) (a) Cassagneau, T.; Fendler, J. H. *Adv. Mater.* **1998**, *10*, 877. (b) Liu, P.; Gong, K.; Ciao, P.; Ciao, M. *J. Mater. Chem.* **2000**, *10*, 933.

(8) Liu, Z.-h.; Ooi, K.; Kanoh, H.; Tang, W.; Tomida, T. *Langmuir* **2000**, *16*, 4154.

(9) Omomo Y.; Sasaki, T.; Wang, L.; Watanabe, M. *J. Am. Chem. Soc.* **2003**, *125*, 3568.

(10) Lan, T.; Kaviratna, P. D.; Pinnavaia, T. J. *Chem. Mater.* **1995**, *7*, 2144.

(11) Abe, R.; Shinohara, K.; Tanaka, A.; Hara. M.; Kondo, J. N.; Domen, K. *Chem. Mater.* **1998**, *10*, 329.

(12) (a) Sasaki, T.; Nakano, S.; Yamauchi, S.; Watanabe, M. *Chem. Mater.* **1997**, *9*, 602. (b) Iida, M.; Sasaki, T.; Watanabe, M. *Chem. Mater.* **1998**, *10*, 3780.

(13) (a) Keller, S. W.; Kim, H.-N.; Mallouk, T. E. *J. Am. Chem. Soc.* **1994**, *116*, 8817. (b) Cassagneau, T.; Fendler, J. H. *Adv. Mater.* **1998**, *10*, 877.

(14) (a) Armstrong, A. R.; Bruce, P. G. *Nature* **1996**, *381*, 499. (b) Armstrong, A. R.; Huang, H.; Jennings, R. A.; Bruce, P. G. *J. Mater. Chem.* **1998**, *8*, 255.

(15) (a) Cao, H.; Suib, S. L. *J. Am. Chem. Soc.* **1994**, *116*, 5334. (b) Skordilis, C. S.; Pomonis, P. J. *Stud. Surf. Sci. Catal.* **1995**, *91*, 513.

10.1021/cm049025d CCC: $27.50
Published on Web 11/20/2004

exhibit new physical and chemical properties that complement those in the bulk. Attempts are being made to prepare nanocrystals of manganese oxide,[15b,18,19] although stable nanoparticles of manganese oxide can be difficult to prepare because of the strong tendency for manganese oxide to precipitate or coagulate during the synthesis. Nanocomposites of pillared layered-manganese oxides can be synthesized by an intercalation process, including the intercalation of organoammonium ions.[20] In 2000, the exfoliation of layered manganese oxide was reported,[8] as a routine synthetic method to induce exfoliation which includes the ion exchange of interlayer alkali metal ions in these layered materials with protons, following by an acid−base reaction of proton-type materials with aqueous solution of organoammonium ions.[21] As a result, the exfoliation/reassembly process has been applied to the synthesis of manganese oxide materials.[22,23] Most recently, Sasaki et al. carried out further intensive study on the intercalation, swelling, and exfoliation of layered manganese oxide.[9] However, the self-assembly behavior of the exfoliated nanosheets has not been reported in detail.

Another use for the self-assembly processes in manganese oxides was found by Suib et al.[18,24a−c] The self-assembly was carried out with stable colloids of lamellar manganese oxide prepared from the reduction of tetraalkylammonium permanganate precursors. An organic cation in the starting sols results in gels that form helices and rings. The self-assembly of manganese oxide mesoporous hollow nanospheres was also reported by this group.[25] However, synthesis at low temperatures through solution-phase reactions by oxidation of Mn^{2+} or reduction of MnO_4^- or redox between these two species generally does not yield a sample with a large crystal size.

It is believed that production of a large-dimension (e.g. micrometer-sized) nanosheet may lead to well-defined swelling and exfoliation behaviors,[9,26] and also, as will be shown in this paper, well-defined self-assembly behavior. We reported last year that single crystals of potassium-type birnessite manganese oxide of around 20 μm in size can be synthesized by a flux method.[27] Herein, we report the use of the single crystals for protonation, exfoliation, and self-assembly behavior investigations. Self-assembly is carried out in a diluted saline aqueous solution, which, we presume, provides an exceedingly mobile environment for nanosheets to "freely" reach a regular or ordered structure according to their crystallographic orientation. The electron-density distribution determined on the basis of structural refinement of the protonated birnessite single crystal is expected to provide information valuable for the understanding of the self-assembly behavior.

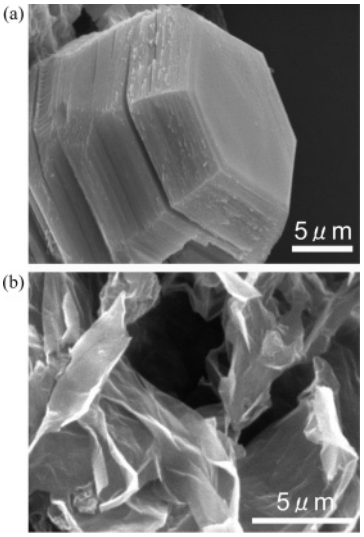

Figure 1. Scanning electron microscope images of (a) protonated birnessite and (b) freeze-dried sample after exfoliation treatment.

Results and Discussion

MnO_2 Nanosheets Prepared by Exfoliation of Protonated Birnessite Crystals. Potassium-type birnessite manganese oxide was protonated through the extraction of potassium ions in a $(NH_4)_2S_2O_8$ aqueous solution at 60 °C. The extraction rate of potassium ions was analyzed as 99.4%, indicating the solution is effective in extracting potassium ions from the crystals. The contents of each element in the H-type birnessite single crystals were analyzed as 9.93 mmol g^{-1} Mn, 18.79 mmol g^{-1} O, and 0.020 mmol g^{-1} K, while the H_2O content was determined to be 7.2 mmol/g by thermogravimetric analysis. Thus, the formula can be written as $H_{0.22}MnO_2 \cdot 0.62H_2O$. A mean manganese oxidation state, Z_{Mn}, of 3.78 is almost the same as that of its K-type precursor (3.75). This result agrees with the result of XPS analysis shown below. Thus, the H/K ion exchange process did not bring about a marked Z_{Mn} change, even when using an oxidative $(NH_4)_2S_2O_8$ solution.

The H-type crystal has a hexagonal prism shape as shown in Figure 1, largely maintaining the morphology

(16) Shen, Y. F.; Zerger, R. P.; DeGuzman, R. N.; Suib, S. L.; McCuidy, L.; Potter, D. I.; O'Young, C. L. *Science* **1993**, *260*, 511.
(17) (a) Mathews, S.; Ramesh, R.; Cenkatesan, T. Benedetto, J. *Science* **1997**, *276*, 328. (b) Tan, G.; Dai, S.; Duan, P.; Zhou, Y.; Lu, H.; Chen, Z. *J. Appl. Phys.* **2003**, *93*, 5480.
(18) Brock, S. L.; Sanabria, M.; Suib, S. L.; Urban, V.; Thiyagarajan, P.; Potter, D. I. *J. Phys. Chem. B* **1999**, *103*, 7416.
(19) (a) Park, S. H.; Sun, Y. K.; Yoon, C. S.; Kim, C. K.; Prakash, J. *J. Mater. Chem.* **2002**, *12*, 3827. (b) Kovacheva, D.; Gadjov, H.; Petrov, K.; Mandal, S.; Lazarraga, M. G.; Pascual, L.; Amarilla, J. M.; Rojas, R. M.; Herrero, P.; Rojo, J. M. *J. Mater. Chem.* **2002**, *12*, 1184. (d) Lu, C. H.; Saha, S. K. *J. Sol−Gel Sci. Technol.* **2001**, *20*, 27. (e) Benaissa, M.; JoseYacaman, M.; Xiao, T. D.; Strutt, P. R. *Appl. Phys. Lett.* **1997**, *70*, 2120.
(20) Wang S.-T.; Cheng, S. *Inorg. Chem.* **1992**, *31*, 1165.
(21) Kaschak, D. M.; Johnson, S. A.; Hooks, D. E.; Kim, H.-N.; Ward, M. D.; Mallouk, T. E. *J. Am. Chem. Soc.* **1998**, *120*, 10887.
(22) (a) Liu, Z.-h.; Ooi, K.; Kanoh, H.; Tang, W.; Yang, X.; Tomida, T. *Chem. Mater.* **2001**, *13*, 475. (b) Liu, Z.-h.; Yang, X.; Makita, Y.; Ooi, K. *Chem. Lett.* **2002**, 680. (c) Xu, Y. H.; Feng, Q.; Kajiyoshi, K.; Yanagisawa, K.; Yang, X.; Makita, Y.; Kasaishi, S.; Ooi, K. *Chem. Mater.* **2002**, *14*, 3844.
(23) (a) Wang, L.; Sasaki, T.; Takada, K.; Kajiyama, A.; Watanabe, M. *Proc. 43rd Battery Symp. (Japan)* **2002**, 58. (b) Wang, L.; Omono, Y.; Sakai, N.; Fukuda, K.; Nakai, I. Ebina, Y.; Takada, K.; Watanabe, M.; Sasaki, T. *Chem. Mater.* **2003**, *15*, 2873.
(24) (a) Giraldo, O.; Marquez, M.; Brock, S. L.; Suib, S. L.; Hillhouse, H.; Tsapatsis, M. *J. Am. Chem. Soc.* **2000**, *122*, 12158. (b) Brock, S. L.; Sanabria, M.; Nair, J.; Suib, S. L.; Ressler, T. *J. Phys. Chem. B* **2001**, *105*, 5404. (c) Veretnnikov, I.; Indeikina, A.; Chang, H.-C.; Marquez, M.; Suib, S. L., Giraldo, O. *Langmuir* **2002**, *18*, 8792. (d) Lvov, Y.; Munge, B.; Giraldo, O.; Ichinose, I.; Suib, S. L.; Rusling, J. F. *Langmuir* **2000**, *16*, 8850.
(25) Yuan, J.; Laubernds, K.; Zhang, Q.; Suib, S. L. *J. Am. Chem. Soc.* **2003**, *125*, 4966.
(26) Miyamoto, N.; Yamamoto, H.; Kaito, R.; Kuroda, K. *Chem. Commun.* **2002**, 2378.
(27) Yang, X.; Tang, W.; Feng, Q.; Ooi, K. *Cryst. Growth Des.* **2003**, *3*, 409.

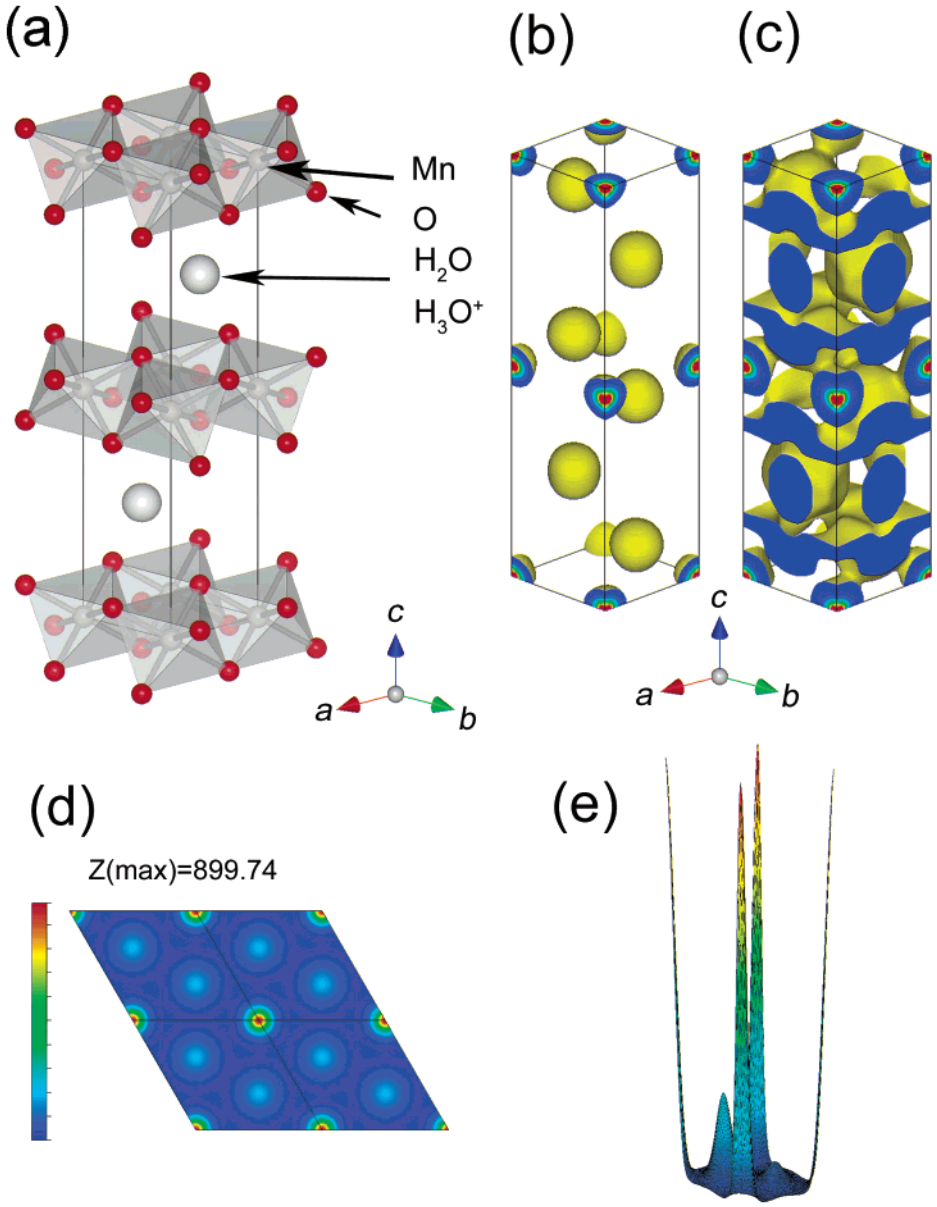

Figure 2. Structural models for protonated birnessite. (a) Crystal structure. Three-dimensional electron-density distribution image, where the isosurface density level is (b) 1.0 and (c) 0.25 $Å^{-3}$. On the incisions (the spectrum form): red, the maximum; blue, the minimum. (d) Two-dimensional map of the (001) plane projected from $z = 0.25-0.75$. (e) Bird's-eye view projected from $z = 0.5-0.75$. The black solid lines indicate the unit cell.

of the K-type crystals except for the lateral faces, which are not as smooth as those of precursor crystal.[27] We have shown elsewhere[27] that the protonated birnessite single crystals have a hexagonal symmetrical structure with space group $P6_3/mmc$. The lattice parameters calculated by a Rietveld refinement are $a = 2.8376(3)$ and $c = 14.4539(5)$ Å. The unit cell is given in Figure 2a. On the basis of the refinement result, the three-dimensional electron-density distribution was visualized (Figure 2b,c). Since the isosurface level is 1 $Å^{-3}$, a regular electron-density distribution can be observed when comparing Figure 2b with Figure 2a. In the unit cell the distribution of the electron density whose isosurface level is 0.25 $Å^{-3}$ concentrates in six layers perpendicular to the *c*-axis: four oxygen (of Mn−O) layers and two water (and/or hydronium) layers. As expected, there is a density layer lower than 0.25 $Å^{-3}$ between an oxygen layer and a water/hydronium layer, which could be considered the base for short-range expansion and subsequent delamination.[8] In each of the four oxygen layers, electron density is not uniformly distributed: around a manganese atom, for example, six high-density hills interspersed with six low-density valleys appear at the range of $z = 0.25-0.75$ (Figure 2d). A bird's-eye view shows the electron density distribution on a side surface of an Mn−O layer in a unit cell (Figure 2e).

The XRD pattern of the wet-state sample obtained by soaking the protonated crystals in TMA^+ hydroxide solution for 10 days consists of a set of basal reflections with $d = 15.65$ Å (Figure 3a). This basal spacing is in concordance with that from the birnessite synthesized by precipitation[8] but remarkably different from the TMA^+-type birnessite prepared by a sol−gel process.[28]

(28) Giovanoli, R. In *Manganese Dioxide Symposium* (Tokyo, 1980); Schumm, B., Jr., Joseph, H. M., Kozawa, A., Eds.; I. C. MnO_2 Sample Office: Cleveland, OH, 1981; Vol. 2, p 97.

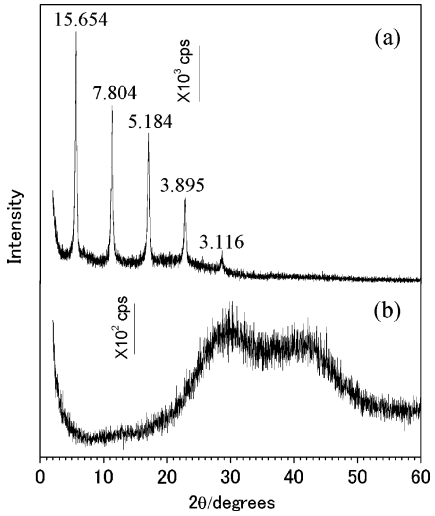

Figure 3. X-ray diffraction patterns of the samples in wet state: (a) after H-type birnessite soaked in TMAOH solution for 10 days and (b) with subsequent water-washing several times.

Because the 15.65 Å basal spacing means TMA^+ ions with bilayer hydrate exist in the interlayer, the obtained sample should be more precisely called buserite,[28] rather than birnessite, which has monolayer water in the interlayer. Note that drying at 70 °C removed part of the water, converting the TMA-type buserite to TMA-type birnessite with a basal spacing of 9.6 Å.

After the TMA-type buserite was water-washed 4 times, a broad halo on the XRD pattern was observed, as shown in Figure 3b. This pattern illustrates the exfoliation of the sample. Figure 1b is the scanning electron microscopy (SEM) image of the freeze-dried sample. As shown, the particles are less than 0.1 μm in thickness and wrinkles and folds are observed on lettuce leaf-like particle surfaces, indicating that the particles are flexible. The diameter of the particle agrees with the original size, as shown in Figure 1a, indicating the exfoliation process undergone did not cause the plane of the MnO_2 framework to fragment in the course of the experiment. The atomic force microscopy (AFM) image (Figure 4) of the sample in the supernatant of the suspension confirms the thickness of the sheet is about 0.7 nm, indicating that the MnO_2 nanosheet is unilamella. Figure 5 is the transmission electron microscopy (TEM) micrograph and selected area electron diffraction (SAED) pattern on the sample. As shown in Figure 5, large nanosheets could be observed, and the SAED pattern shows a pattern of single crystals.

Self-Assembly of the MnO_2 Nanosheets. By treating the colloidal suspension of nanosheets in a dilute NaCl solution, after which it was water-washed and dried, a self-assembled sample was obtained. Figure 6 gives the SEM image of the sample. The particles show a bulk plate, different from that of the freeze-dried exfoliated sample (Figure 1b). On the surface, plate morphology can be clearly observed, similar to that usually reported for precipitated and hydrothermally treated birnessite samples with good crystallinity.[8,22] This morphology implies that the present self-assembled sample is well-restacked. The XRD pattern of the sample is given in Figure 7. Two peaks at $d = 7.23$ and 3.61 Å are observed to be stronger than the other peaks

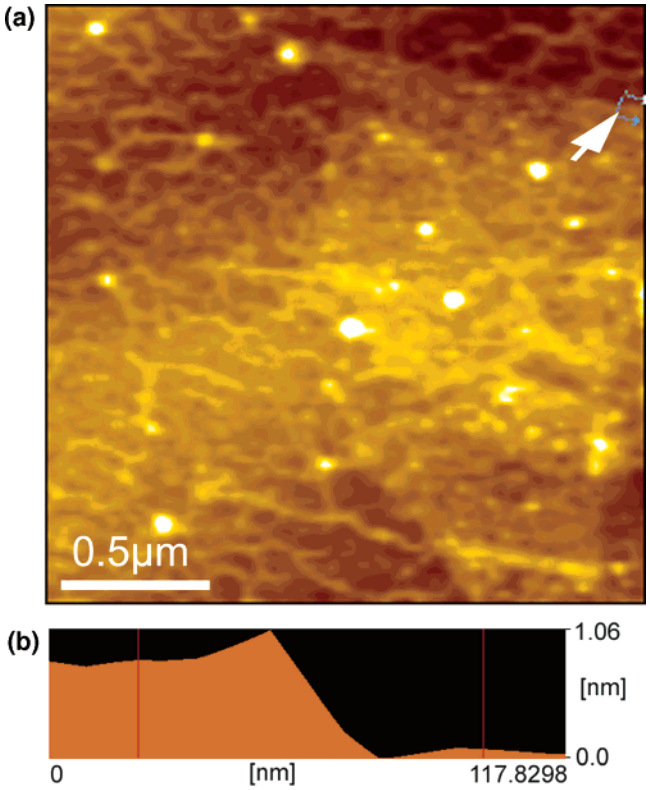

Figure 4. Tapping-mode atomic force microscopy image (a) of manganese oxide nanosheets deposited on PEI precoated silicon wafer. The arrow indicates the range used to measure the thickness, shown in b, giving an average thickness of 0.72 nm.

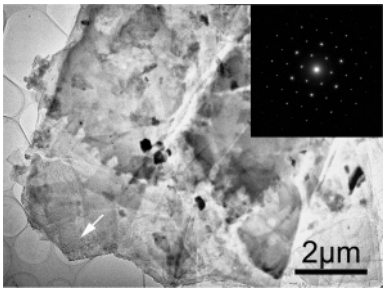

Figure 5. TEM micrographs and selected electron diffraction pattern of manganese oxide nanosheets.

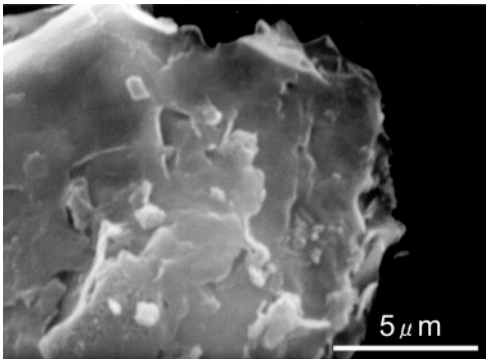

Figure 6. Scanning electron microscope images of the self-assembled sample.

in the pattern. These two peaks and the peaks at $d =$ 2.41, 1.80, 1.19, 1.03, and 0.90 Å in the region of $2\theta >$ 30° compose a set of basal reflections with d values corresponding to a minimum periodicity along $c = 7.23$

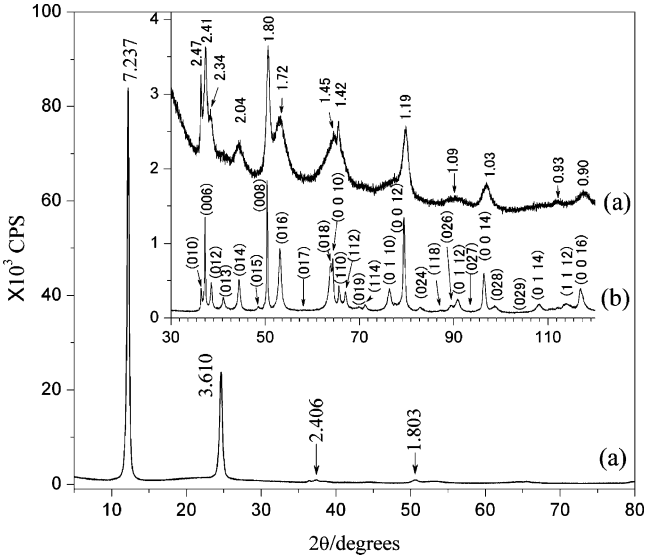

Figure 7. X-ray diffraction patterns of (a) the self-assembled sample compared with (b) H-type birnessite. *d* values are in angstroms; plane indexes in b according to the hexagonal symmetry structure with space group $P6_3/mmc$ by a Rietveld refinement.[27]

Å. The pattern confirms that the nanosheets are restacked yielding a phase of layered manganese oxide. Chemical analysis showed that the sample had the composition, $H_{0.18}Na_{0.089}MnO_2 \cdot 0.47H_2O$ ($Z_{Mn} = 3.73$). The sodium ions in the interlayer of the layered compound result in the basal spacing being slightly smaller than protonated birnessite. This basal spacing implies that TMA^+ was replaced during the assembly process. This is confirmed by infrared spectroscopy (shown below). This result is different from those obtained by the conventionally dried route,[8,9] where several kinds of layered manganese oxide phases with different basal spacing were formed due to the residual tetraalkylammonium ions.

Comparing Figure 7a with Figure 7b, the peaks of Figure 7a could be indexed to the same hexagonal symmetry as that of H-type birnessite. The calculated unit cell parameters are estimated as $a = b = 2.84$ Å, $c = 14.41$ Å. All the 00*l* reflections are sharp, whereas the peaks of other diffraction indices are rather broadening and overlapped, e.g. at 2θ about 65−70° and about 90°. The probable reason for the powder pattern is that in the [00*l*] directions, i.e. along the *c*-axis, the nanosheets are restacked regularly, but in the other directions the crystallinity is low.

The TEM micrograph for the reassembled sample is shown in Figure 8. A polycrystal-like SAED pattern for the sample is seen (Figure 8b). From the six brightest spots of the hexagonal reciprocal lattice as shown in Figure 8b′, the lattice parameters were estimated. The result illustrated that the incidence of the electron beam was along the [001] direction and the obtained parameter values ($a = b = 2.78$ Å) coincide well with those from the X-ray diffraction (XRD) result. As shown in Figure 8b, the ringlike pattern consists of at least four sets of hexagonally distributed spots. When we inclined the sample, the following SAED pattern changes could be observed. First, as shown in Figure 8b, the relative brightness between the spot sets does not change; that is, the spots are deduced from the same zero-order Laue

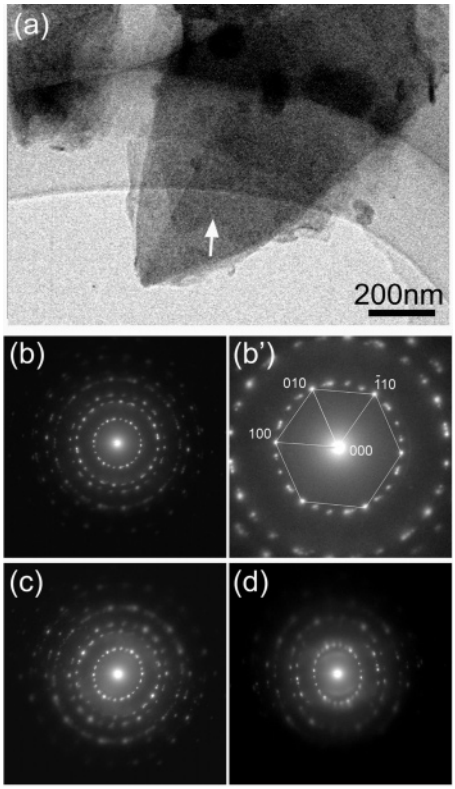

Figure 8. TEM micrograph (a) of the self-assembled sample, and SAED patterns collected from the sample inclined to the following: (b and b′) $x = 0°$, $y = 0°$; (c) $x = 12°$, $y = 0°$; and (d) $x = 0°$, $y = -20°$.

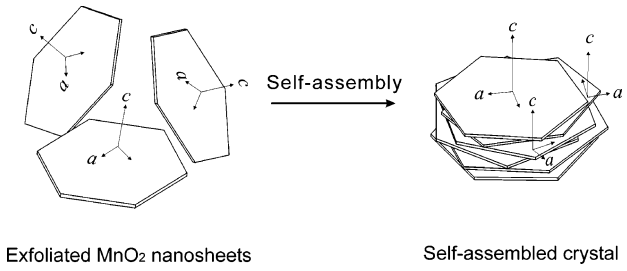

Figure 9. Proposed schematic model for (a) exfoliated and (b) reassembled birnessite.

zone. Second, the elliptic patterns can be observed in Figure 8c,d. The elliptic patterns signify the existence of the fiber axis at the thin film sample.[29] The direction of the fiber axis is the same as that of the *c*-axes, because the circle pattern showed the [001] incidence direction.

A proposed model for the reassembled birnessite is given in Figure 9. The exfoliated nanosheets reassemble to a so-called "textured polycrystalline structure", where the nanosheets have *c*-axes aligned along a certain direction, i.e. the fiber axis direction, while the *a*- or *b*-axis of each nanosheet is azimuthally orientated about the *c*-axis. Each spot in the SAED pattern has the intensity distribution parallel to the *c**-axis in the reciprocal plane and becomes a streak in length inversely proportional to thickness when the thickness of a specimen is so small.[29] The spot sets form an ellipse when the beam is at an angle to the fiber axis, whereas

(29) Hirsch, P. B.; Howie, A.; Nicholson, R. B.; Pashley, D. W.; Whelan, M. J. *Electron Microscopy of Thin Crystals*, Reprinted and Revised; Butterworth: London, 1967; p 116,

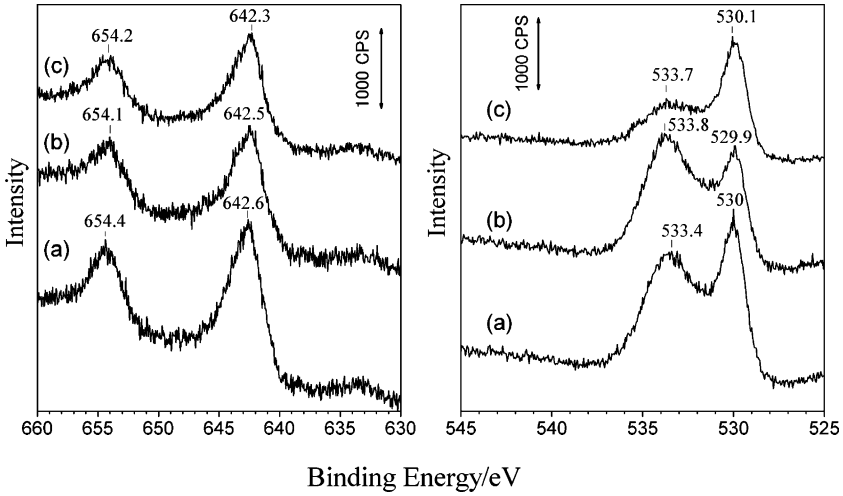

Figure 10. X-ray photoelectron spectroscopy spectra of (a) K-type, (b) H-type, and (c) the self-assembled birnessite crystals.

the spot sets appear to lie in a circle when the electron beam is parallel to the fiber axis. In the model (Figure 9), the nanosheets with approximate diametral dimensions were assumed to stack upon each other. Another possibility is that some small sheets stack on a large surface of nanosheet, as we proposed for a nanocomposite where small birnessite layers stack on a large graphite oxide surface.[30] Each of the two stacking layers would give an elliptic SAED pattern. We assume that the former is the main in the present case, since the relatively uniform size of the starting crystals was observed by SEM. This model can be applied to explain the result of the powder XRD pattern (Figure 7a). Because the orientations of the *a*- or *b*-axes are different in the individual nanosheets, the reflections referring to the two axes would show low crystallinity.

Four types of self-assembly are proposed: static, dynamic, templated, and biological self-assembly.[1] Atomic, ionic, and molecular crystals belong to the static type.[31] The reassembly of negatively charged manganese oxide nanosheet can be attributed to this type also. Equilibration is usually required to reach ordered structures. In the potassium-type birnessite crystal growth in a flux, the components are K, Mn, and O ions. They adjust their positions to form a single crystal. When the components or building blocks are negatively charged nanosheets, and Na and H cations, to form a regular structure may be more difficult than when only those K, Mn, and O ions do, because energetically the activation energy to reorient a large sheet, once it has attached to another sheet (in the wrong orientation), must be large. This can explain the formation of a fiber axis. On the other hand, the SAED pattern is not a ring but several sets of spots belonging to one sheet or several sheets with the same direction of *a*- or *b*-axis. Our observations on the sample did not find a ringed SAED pattern. It means that the orientations of *a*- or *b*-axis may not be a random arrangement but rather lie at particular angles to each other. This arrangement may be related to the electron density distribution as shown in Figure 2 on the nanosheet surfaces and their interaction with the cation species during assembly. Whether the particular angles of the *a*- or *b*-axis of individual nanosheets results in the lower energy of the system or whether they adjust their angle to that in a single crystal needs further study.

Characterizations. In the XPS spectrum of the potassium-type birnessite crystals, the Mn 2p region consisted of a spin−orbit doublet with an Mn ($2p_{1/2}$) having a binding energy of 654 eV and an Mn ($2p_{3/2}$) with a binding energy of 642.3 eV (Figure 10).[32a] This doublet can be assigned to a mixed-valent manganese system,[32b] most likely Mn^{4+} and Mn^{3+}.[24d] The O 1s region showed two peaks at 533 and 530.0 eV. They indicate the different chemical environments for the oxygen atoms. The lower binding energy peak at 530 eV is oxide (O^{2-}), while a spectral fitting for birnessite manganese oxide revealed that the higher binding energy peaks is H_2O and the peak at intermediate binding energy existed between the oxide and H_2O peaks is OH^-.[32b] As shown in Figure 10b, the 534 eV peak of the H-type birnessite becomes higher than that of the 530 eV peak. This is consistent with the sample having more water and OH^- than that of K-type birnessite. The self-assembled birnessite shows the 534 eV peak with low intensity (Figure 10c) due to sodium ions instead of protons in the interlayers.

The doublet of Mn 2p and the 530 eV peak of K-type birnessite did not shift noticeably in the protonated (Figure 10b) and self-assembled (Figure 10c) birnessite crystals, and the peak shape did not show marked change. It implies that the mean oxidation state of manganese does not remarkably change. This is consistent with the chemical analysis result of mixed-valent manganese oxide crystals, 3.73−3.78. Previous work showed that the oxidation state of manganese remains unchanged during an exfoliation and subsequent layer-by-layer restacking process.[23b] The present XPS observation suggests that the average oxidation state of manganese is stable during the protonation, exfoliation, and self-assembly process.

(30) Yang, X.; Makita, Y.; Liu, Z.-h.; Ooi, K. *Chem. Mater.* **2003**, *15*, 1228.

(31) (a) Philip, D.; Stoddart, J. F. *Angew. Chem., Int. Ed. Engl.* **1996**, *35*, 1155. (b) Isaacs, L.; Chin, D. N; Bowden, N.; Xia, Y.; Whitesides, G. M. In *Supramolecular Technology*; Reinhoudt, D. N., Ed.; Wiley: New York, 1999; pp 1−46.

(32) (a) Moulder, J. F.; Stickle, W. F.; Sobol, P. E.; Bomben, K. D. In *Handbook of X-ray Photoelectron Spectroscopy*; Chastain, J., Ed.; Perkin-Elmer Corp.; Eden Prairie, MN, 1992. (b) Banerjee, D.; Nesbitt, H. W. *Geochim. Cosmochim. Acta* **2001**, *65*, 1703.

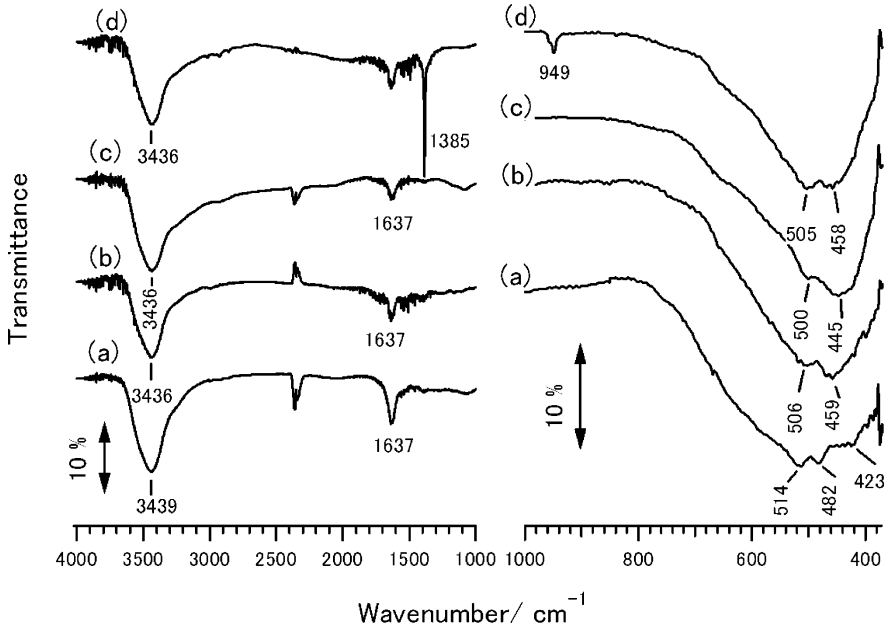

Figure 11. IR spectra of (a) K-type, (b) H-type, (c) self-assembled birnessite, and (d) an exfoliated sample restacked, placed on a glass substrate, and dried at room temperature.

The FT-IR spectra of the potassium-type, protonated, and the self-assembled birnessite are shown in Figure 11. The bands around 3439 and 1637 cm^{-1} are recognized as being due to the stretching and bending vibrations of water molecules or hydroxyl groups in the interlayer.[33] The existence of the interlayer water or hydroxyl groups in the K-type birnessite single crystals (Figure 11a) agrees with the basal spacing of 7.12 Å, because the K-type birnessite as prepared in the flux without water-washing had a basal spacing of 7.05 Å. No vibration band concerning TMA^+ can be found in the spectrum of the self-assembled sample (Figure 11c), while the two bands at 1385 and 949 cm^{-1} in the spectrum of the conventionally dried sample (Figure 11d) are assigned to the absorption of TMA^+ ions in the solid.[34]

In the range of less than 700 cm^{-1}, 514, 482, and 423 cm^{-1} bands can be observed for K-type birnessite (Figure 11a). The two former bands corresponding to Mn−O stretching vibrations are characteristic IR bands in birnessite.[35] The protonation of the sample causes a marked change in this range, as shown in Figure 11b; only two bands at 506 and 459cm^{-1} appeared in the spectrum of the sample. Furthermore, for the self-assembled birnessite they changed to 500 and 445 cm^{-1} (Figure 11c). The most likely explanation is that the two birnessite-characteristic bands shift to a low wavenumber due to an increase of the Mn−O band strength in the protonated birnessite, resulting in an overlap of 482 and 423 cm^{-1}. This influence becomes more intense in the self-assembled birnessite.

The thermogravimetric and differential thermal analysis (TG-DTA) curves of the three samples are plotted in Figure 12. For the K-type birnessite, two endothermic peaks at lower than 100 and 164 °C (Figure 12a) are due to the evaporation of physisorbed water and the dehydration of birnessite. Correspondingly, in the TG curve weight losses are observed until about 400 °C. For the H-type and self-assembled birnessite (Figure 12b,c), the weight loss due to dehydration is shown more clearly, whereas endothermicity is not as sharp as that for K-type birnessite. In Figure 12b, an endothermic peak at 549 °C for the H-type birnessite with a large weight loss is caused by oxygen release, which corre-

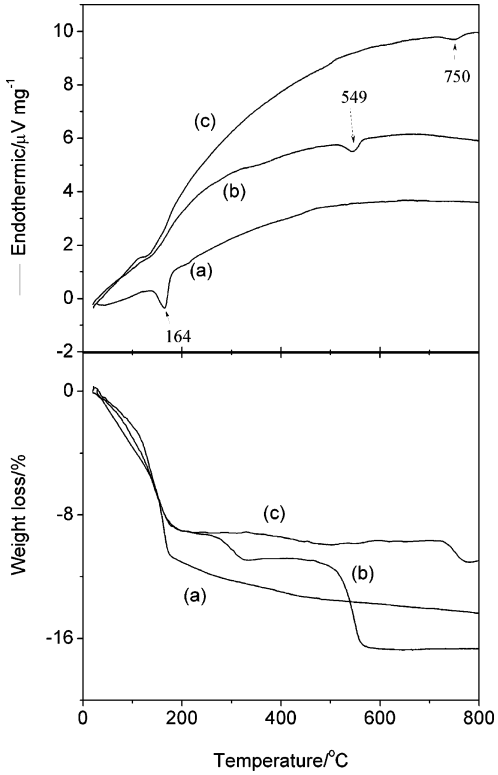

Figure 12. Plots of the TG and DTA analysis of the samples: (a) K-type, (b) H-type, and (c) self-assembled birnessite.

(33) (a) Ryskin, Y. I. In *Mineralogical Society Monograph 4*; *The Infrared Spectra of Minerals*; Farmer, V. C., Ed.; Mineralogical Society: London, 1974; p 154. (b) Yang, D. S.; Wang, M. K. *Chem. Mater.* **2001**, *13*, 2589.

(34) Kooli, F. *J. Mater. Chem.* **2002**, *12*, 1374

(35) (a) Potter, R. M.; Rossman, G. R. *Am. Mineral.* **1979**, *64*, 1199. (b) Luo, J.; Huang, A.; Park, S.; Suib, S. L.; O'Young, C. L. *Chem. Mater.* **1998**, *10*, 1561.

sponds to the reduction of tetravalent manganese.[36] This endothermic peak and weight loss cannot be clearly observed in the curves of the K-type and self-assembled samples. It may imply that a small amount of sodium ions in the interlayer could stabilize the birnessite structure.

Conclusions

The protonated birnessite single crystals with hexagonal symmetry ($a = 2.8376(3)$ Å, $c = 14.4539(5)$ Å) can be exfoliated to MnO_2 unilamellar nanosheets by a TMA^+/H^+ ion-exchange and subsequent water-washing. The self-assembly of exfoliated MnO_2 nanosheets in a dilute NaCl solution produced layered crystals with basal spacing of 0.72 nm. The resulting layered crystal had a textured polycrystalline structure, in which *c*-axes of the nanosheets aligning along a certain direction constitute a fiber axis with azimuthal orientations of *a*- or *b*-axes about the fiber axis. No ring SAED pattern was observed on the layered crystals. This probably implies that azimuthal orientations of *a*- or *b*-axes are not random. We assume that the angles of the *a*- or *b*-axes relate to the electron-density distribution on the exfoliated nanosheets and their interaction with cation species when assembling. The mean oxidation state of manganese exhibits no marked change during the protonation, exfoliation, and self-assembly process.

Experimental Section

Starting Materials. The starting material, single crystals of K^+-form birnessite manganese oxide, was prepared by a flux method reported elsewhere.[27] A mixture of γ-MnOOH (5 g) and KNO_3 (25 g) was heated in a 200 mL crucible at 700 °C for 24 h.

Potassium ions were extracted from the sample (2 g) using a 0.5 M $(NH_4)_2S_2O_8$ aqueous solution (500 mL) at 60 °C for 7 h. The solid was filtered, washed with ion-exchanged water for several times, and then dried at 70 °C overnight. The extraction rate of K^+ was analyzed as 99.4%. By comparison, using 0.1 M HCl aqueous solution and refreshing the solution daily for 12 days, the extraction rate was 93.0%.

TMA^+-Intercalation and Exfoliation. Using the method previously reported,[8] weighed protonated birnessite sample (1 g) was soaked in a 0.35 M tetramethylammonium (TMA^+) hydroxide aqueous solution (250 mL) and stirred at room temperature for 10 days. The sample was centrifuged and then water-washed and subsequently centrifuged for 4 times. The water-washing caused the TMA^+ intercalated samples to exfoliate.[8]

Self-Assembly. The self-assembly of the exfoliated birnessite sheets was carried out using a dialysis/salting-out method. The dark-brown-colored colloidal suspension containing about 0.2 g of birnessite was diluted and put into molecular-porous dialysis membrane tubing (Spectra/Por 4; MWCO, 12 000−14 000). The tubing was soaked in a 10^{-3} M NaCl aqueous solution (2 L). The aqueous saline solution was replaced with a new one every 24 h. After soaking for 10 days, the supernatant solution became colorless and clear. The precipitate was filtered, water-washed, and dried at 70 °C for 12 h. For comparison, the exfoliated suspension was set on a glass substrate and conventionally dried in air at room temperature.

Chemical Analysis. K, Na, and Mn contents were determined by atomic absorption spectrophotometry (Shimadsu AA670) after dissolving the samples in a mixed solution of HCl + H_2O_2. The mean valency of Mn was obtained by standard titration with oxalic acid.[37] The water content was estimated from the weight loss by heating to 400 °C.

Instrumentation. Powder XRD patterns were collected using a Rigaku RINT 2100 diffractometer with Cu K_α radiation.

TEM and SAED observation was performed using a JEOL, JEM-3010 transmission electron microscope at an accelerating voltage of 300 kV. The samples were supported on microgrids. SEM observations were carried out in a JEOL type JSM-5310 scanning electron microscope.

A JSPM-5200 scanning probe microscope was employed to obtain a topographical image of the nanosheets. Samples were prepared by dropping the diluted suspension onto a silicon wafer (on which polyethylenimine (PEI) was precoated), and then air-dried.

Thermogravimetric and differential thermal analysis data were collected in a MAC Science thermal analyzer, system 001 TG-DTA 2000 with a heating rate of 10 °C/min.

Infrared spectra of the samples were recorded on a Perkin-Elmer infrared spectrometer, 1600 Series FTIR using the KBr method.

XPS measurements were performed with an ESCA-1000 spectrometer (Shimadzu) using Mg K_α (1253.6 eV) radiation at a power of 200 W (20 mA and 10 kV). The vacuum of the analysis chamber was higher than 2×10^{-8} Pa. A Ag conducting specimen was used as the binding energy standard to ensure the accuracy of the data measured. The doublet of Ag $3d_{3/2}$ and $3d_{5/2}$ was detected, where the $3d_{5/2} = 368.3$ eV, in close agreement with that of ref 32a.

Calculation of Electron-Density Distribution. Electron-density distribution in protonated crystal was visualized by whole-pattern fitting based on the maximum entropy method (MEM),[38a] from the obtained XRD pattern, using the RIETAN-2000 and PRIMA softwares.[38b] Three virtual chemical species were introduced into the refinements, W1, whose atomic scattering factor is the sum of one O and two H atoms, W2, with one O and three H atoms, and M, with 0.77 Mn^{4+} and 0.23 Mn^{3+}, corresponding to the oxidation state of Mn. The contents of W1 and W2 were determined by the compositional formula, $H_{0.22}MnO_2 \cdot 0.62H_2O$. W1 and W2 were set to occupy the 2d site in the space group $P6_3/mmc$; M, to 2a; and O, to 4f, whose $x = 1/3$, $y = 2/3$, and $z = 0.0704(2)$ as calculated. The independently observed structure factors of F_o(Rietveld) were estimated from the XRD data on the basis of refined parameters. The *R*-factors ($R_{wp} = 0.1039$, $R_p = 0.0751$, $R_R = 0.1553$, $R_e = 0.0373$) showed the refinement is better than that we reported before.[27] The temperature factor *B* is 4.7(2), 1.84(5), or 0.37(4) Å^2 for H_2O (and H_3O^+ (whose B is set as the same as that of H_2O), O, or Mn, respectively. In the MEM analysis, the unit cell was divided into $64 \times 64 \times 128$ pixels. The three-dimensional electron-density distribution and crystal structure models were visualized with VINUS software.[38b]

Supporting Information Available: Rietveld refinement plots for the protonated birnessite manganese oxide (PDF). This material is available free of charge via the Internet at http://pubs.acs.org.

CM049025D

(36) Feng, Q.; Kanoh, H.; Miyai, Y.; Ooi, K. *Chem. Mater.* **1995**, *7*, 1722.

(37) JIS N8233. *Methods for Determination of Active Oxygen in Manganese Ores*; Japanese Industrial Standards Committee: Tokyo, 1969.

(38) (a) Izumi, F.; Kumazawa, S.; Ikeda, T.; Hu, W.-Z.; Yamamoto, A.; Oikawa, K. *Mater. Sci. Forum* **2001**, *378*−*381*, 59. (b) Izumi, F. http:// homepage.mac.com/fujioizumi/index.html.